XIV International Conference on Computational Plasticity. Fundamentals and Applications
COMPLAS 2017
E. Oñate, D.R.J. Owen, D. Peric and M. Chiumenti (Eds)

COMPARISON OF GURSON AND LEMAITRE MODEL IN THE CONTEXT OF BLANKING SIMULATION OF A HIGH STRENGTH STEEL

FLORIAN GUTKNECHT, KERIM ISIK,

TILL CLAUSMEYER AND A. ERMAN TEKKAYA

Institute of Forming Technology and Lightweight Construction (IUL)
Technical University Dortmund
Baroper Str. 303, 44227 Dortmund, Germany
Email: Florian.Gutknecht@iul.tu-dortmund.de, www.iul.eu

Key words: sheet metal, blanking, damage model, parameter identification, simulation.

Abstract. The process of blanking takes place in a short band with high accumulated strain undergoing various stress triaxialities. Enhanced implementations for shear and compressive loads of Gurson's and Lemaitre's model are directly compared for the same blanking setup. For a dual phase steel DP600 the Lemaitre parameters are identified completely by an inverse strategy, while the parameters of the Gurson's porous plasticity model are predominantly gained from analysis with a scanning electron microscopy (SEM). The models are validated by comparison of force-displacement curves, time point and location of crack initiation. Advantages and disadvantages of both approaches are discussed with respect to prediction accuracy and costs of parameter identification. Both of the models deliver an exact prediction for the location of the crack and a good prediction of the punch displacement at the onset of cracking.

1 INTRODUCTION

In recent decades, numerous improvements of early damage models have been made. Research in this field follows basically two different approaches. On the one hand, there are microscopicly motivated damage models which go back to the idea of Gurson [1], Tvergaard and Needleman [2]. These are referred to as "porous plasticity", as the measure for material degradation is the void volume fraction, which leads to softening due to this degradation. On the other hand, there are phenomenological models (e.g. Lemaitre [3]) which are often derived within the context of thermodynamics. As these models are not linked to microstructure the quantity associated to material degradation is an internal variable called "damage" instead of a void volume fraction. As most internal variables in thermodynamics, the "damage" is not necessarily directly measureable as void volume fraction. Thus coefficients in the evolution equations (e.g. material parameters) must be determined via inverse parameter identification.

Both approaches need intense amount of effort for parameter identification. The microscopically motivated models need several hours of scanning electron microscopy (SEM) and an experienced operator to obtain meaningful and reliable results. The phenomenological models need a series of different experiments and computing capacity for inverse identification.

As a consequence it is of significant interest for users, as well as researchers in this field to have some comparative results to identify the advantages and disadvantages of both approaches.

Vaz et al. [4] recently compared modern implementations of Lemaitre and Gurson models, but focused on identification strategy and finally applied the models to uniaxial tension. Hambli [5] compared basic versions of Lemaitre and Gurson models in the context of blanking. He found the Lemaitre model to yield better predictions in terms of crack initiation and propagation. Since then several modifications for the Gurson model have been proposed. Nahshon and Hutchinson [6] suggested to add a term for void growth due to shear load. This enhanced porous plasticity model is used by the authors in [7] for the simulation of a blanking process. Along the way further modifications for Lemaitre's model have been proposed. Desmorat and Cantournet [8] suggested a modification to consider the effect of negative triaxialities. A similar approach presented by Soyarslan and Tekkaya [9] to account for the coupling of orthotropic plasticity and damage is used by the authors in [10] for the simulation of a blanking process. As both studies had different purposes they had different setups and focused on different aspects for validation. In this study, both approaches are directly compared for the same blanking setup.

The following section briefly introduces the experiments and microscope analysis that are necessary for the comparison. Section 3 addresses the aspects of simulation (i.e. material model and parameter identification). In section 4, the simulation results are compared to the experimental data and discussed. The paper ends with a conclusion in section 5.

2 EXPERIMENTS

After a brief summary of the investigated material the setup of experiments for parameter identification and process validation are presented in section 2.1. Section 2.2 briefly describes how material parameters for Gurson model were measured. The material investigated is a dual phase steel, DP600 with a thickness of 2 mm. The chemical composition and basic mechanical properties measured in standard tensile test are given in Table 1.

Table 1: Mechanical properties from uniaxial test and chemical composoition of DP600.

Modulus of Elasticity in MPa	**Poisson's ratio**	**Anisotropy**			**Yield strength in MPa**	**Swift hardening (eq. 3.4)**		
		r_0	r_{45}	r_{90}		K *in* MPa	e_0	n
201400	0.3	0.974	0.972	1.217	359	983	0.00232	0.190

C	**Mn**	**Cu**	**Ni**	**P**	**Cr**	**Mo**	**Al**	**Ti**	**S**	**Si**	**Fe**
0.081	1.45	0.056	0.071	0.021	0.212	0.00	0.029	0.002	0.005	0.255	balance

2.1 Tests (Macro level)

For this study, three experiments are necessary. Notched tensile tests and biaxial Nakajima tests are conducted for parameter identification and blanking tests are run in a universal testing

machine for validation. The notched tensile tests have a twofold use. On the one hand, they are used for direct measurement of void volume fraction and void nucleation in the Gurson model (section 2.2) and on the other hand, they are used for inverse identification of the Lemaitre model parameters (section 3.3). The notched tensile specimen has a width of 20 mm and length of 235 mm. Notches with a radius of 10 mm are cut with a laser from both sides at the centre of the long side. Thus the minimum width is 10 mm. The specimens are elongated with a constant strain rate of 0.0025 s^{-1}. The displacement field in the notched area is captured with optical camera system GOM Aramis. The biaxial specimen is one of the Nakajima geometries used for the identification of forming limit curve. Standard DIN EN ISO 12004-2 defines the specimen geometries and testing methodology for forming limit curves. Testing setup consist of the hemispherical punch with radius of 50 mm, blankholder and die. The circular blank without any notch has a radius of 100 mm and results in the deformation path close to equibiaxial deformation till necking. The force-displacement curves taken from the experiments are used as the objective function for the inverse parameter identification methodology. The test is conducted till final fracture to cover forming behaviour beyond necking.

The blanking experiments were conducted with a punching module (Figure 1) that is attached to universal testing machine Zwick 250. Thus intermediate stops of the punch are possible and the force and displacement of the punch can be recorded for validation. The cylindrical punch has radius of 8 mm. The tip of punch and die have edge radii of 25 µm. The cutting clearance is 80 µm, which corresponds 4% of sheet thickness.

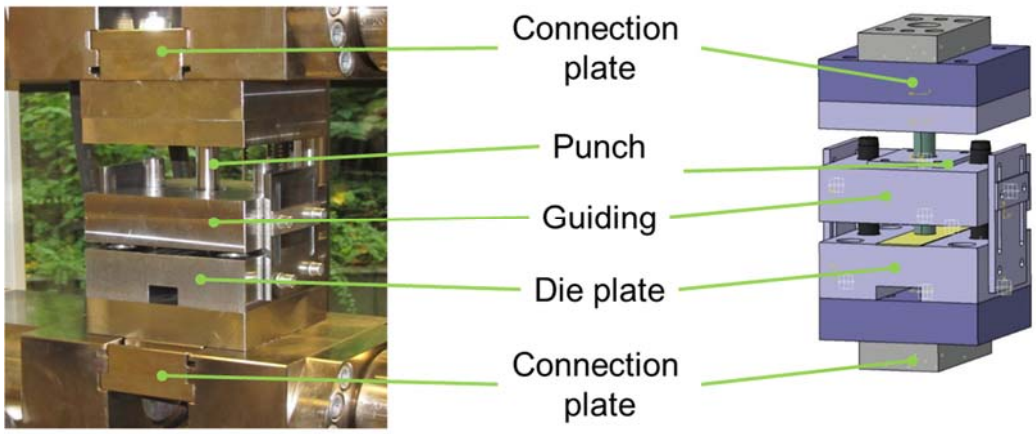

Figure 1: Punching module (left) and schematic representation (right) used for validation of blanking process simulation.

2.2 Tests (Micro level)

The samples for micrographs are detached with a precision cut-off machine. Afterwards an ion-etch-system is used to prepare the samples' surface by using ion beam slope cutting. With this method, it is possible to observe voids with an area as small as 0.05 µm². Details of the method are presented in [11]. This approach makes it possible to directly quantify the initial void volume fraction f_0 assuming that the void volume fraction approximately equals the void area fraction and thus can be obtained by the ratio of surface area of the voids to the total area of that surface. Furthermore, the method proposed in [12] makes it possible to identify the

parameters for void nucleation f_N, S_N and e^p_N (cf. eq. 3.9) with the analysis of a notched tensile specimen. Therefore one half of the notched region is divided into eight zones. Each of these zones corresponds to a certain equivalent plastic strain and has a characteristic mean void size. The voids having a smaller size than the mean size of the neighbouring zone, which has a lower deformation is counted as newly nucleated void for that zone. Thus one gets a uniform distribution of nucleated void volume fraction and can fit the parameters to that distribution (Table 2).

3 SIMULATIONS

This section starts with an introduction to the common framework of both materials models used. Afterwards characteristics of the used Gurson and Lemaitre type models are given. Section 3.2 presents the model setup of the blanking process and experiments for inverse identification. This section closes with information about the numerical identification strategy.

3.1 Material models

Both material models in this study fall in the context of continuum damage mechanics. The framework uses a multiplicative split of the total deformation gradient

$$\mathbf{F} = \mathbf{F}^{\mathrm{e}} \bullet \mathbf{F}^{\mathrm{p}} \tag{3.1}$$

into elastic $\mathbf{F}^{\mathrm{e}}$ and plastic part $\mathbf{F}^{\mathrm{p}}$ as proposed by Lee [13]. The kinematic formulation of the model relies on an approximation for the logarithmic, elastic stretch $\mathbf{U}^{\mathrm{e}}$, which arises in the context of the polar decomposition $\mathbf{F}^{\mathrm{e}} = \mathbf{R}^{\mathrm{e}} \bullet \mathbf{U}^{\mathrm{e}}$, with $\mathbf{R}^{\mathrm{e}}$ the elastic rotation tensor. As demonstrated in [14] one obtains

$$\frac{d}{dt}\ln(\mathbf{U}^{\mathrm{e}}) = \mathbf{R}^{\mathrm{e}} \bullet \mathbf{D} \bullet \mathbf{R}^{\mathrm{e}\mathrm{T}} - \mathbf{D}^{\mathrm{P}} \tag{3.2}$$

$$\dot{\mathbf{R}}^{\mathrm{e}} = \mathbf{W} \bullet \mathbf{R}^{\mathrm{e}} - \mathbf{R}^{\mathrm{e}} \mathbf{W}^{\mathrm{P}} \tag{3.3}$$

for small elastic strain, i.e. $|\ln(\mathbf{U}^{\mathrm{e}})| << 1$. The rate of total deformation $\mathbf{D} = \mathrm{sym}(\mathbf{L})$ is given in terms of the "velocity gradient" $\mathbf{L} = \dot{\mathbf{F}}^{\mathrm{p}} \bullet \mathbf{F}^{-1}$. Consequently, $\mathbf{D}^{\mathrm{p}} = \mathrm{sym}(\mathbf{L}^{\mathrm{p}}) = \mathrm{sym}(\dot{\mathbf{F}}^{\mathrm{p}} \bullet \dot{\mathbf{F}}^{-1})$ and $\mathbf{W}^{\mathrm{p}} = \mathrm{skw}(\mathbf{L}^{\mathrm{p}})$ represent the rate of plastic rotation and the plastic spin, respectively. The assumption $\mathbf{W}^{\mathrm{P}} \approx \mathbf{0}$ is justified for the investigated metals, such that the material axes rotate with the continuum. The associative flow rule

$$\mathbf{D}^{\mathrm{P}} = \dot{\gamma} \partial_{\mathbf{T}} \Phi^{\mathrm{P}} \tag{3.4}$$

determines the rate of plastic deformation depending on the specific choice of the yield function Φ^{P} and the magnitude of the plastic multiplicator $\dot{\gamma}$. The Cauchy stress tensor is denoted by $\mathbf{T}$, and its principal stresses are T_i. Stress triaxiality is defined as $\eta = -p/\sigma_{\mathrm{eq}}$ with hydrostatic pressure $-p = \sigma_{\mathrm{m}} = 1/3\,\mathrm{tr}[\mathbf{T}]$ and equivalent von Mises stress σ_{eq}. The next paragraph presents a short summary of the coupled elasto-plastic damage models used in this comparative study.

Enhanced Gurson Model

The yield function of the Gurson model has the general form:

$$\Phi^{P} = \left(\frac{\sigma_{\mathrm{eq}}}{\sigma_{\mathrm{y}}}\right)^{2} + 2q_1 f^{*} \cosh\left[\frac{3}{2}\frac{q_2\sigma_{\mathrm{m}}}{\sigma_{\mathrm{y}}}\right] - (1 - q_3 f^{*2}) = 0 \tag{3.5}$$

where q_1, q_2 und q_3 are material parameters [15], [16] and e^p is the equivalent plastic strain. $\sigma_y = \sigma_y [e^p]$ is the flow stress and for the Swift type isotropic hardening with material parameters K, e_0 und n, it reads:

$$\sigma_{\mathrm{y}}[e^{\mathrm{p}}] = K\,(e_0 + e^{\mathrm{p}})^{n} \tag{3.6}$$

The void volume fraction is modified to f^*, due to the accelerating effects of the void coalescence as follows [2]:

$$f^{*} = \begin{cases} f & f \le f_{\mathrm{c}} \\ f_{\mathrm{c}} + \dfrac{f_{\mathrm{u}}^{*} - f_{\mathrm{c}}}{f_{\mathrm{f}} - f_{\mathrm{c}}}\left(f - f_{\mathrm{c}}\right) & f > f_{\mathrm{c}} \end{cases} \tag{3.7}$$

where critical void volume fraction at incipient coalescence and the void volume fraction at final fracture are denoted by f_c and f_f, respectively. $f_u^*=1/q_1$ is the maximal value of the modified void volume fraction f^* at which the stress carrying capacity vanishes macroscopically. This corresponds to the trigger for the element deletion to model fracture.
The change in the void volume fraction $\dot{f}$ has contributions due to the nucleation of the new voids $\dot{f}^{\mathrm{n}}$, void growth due to hydrostatic stresses $\dot{f}^{\mathrm{g}}_{\mathrm{hyd}}$ and void growth due to the shear stresses $\dot{f}^{\mathrm{g}}_{\mathrm{shr}}$:

$$\dot{f} = \dot{f}^{\mathrm{n}} + \dot{f}^{\mathrm{g}}_{\mathrm{hyd}} + \dot{f}^{\mathrm{g}}_{\mathrm{shr}} \tag{3.8}$$

The nucleation of the voids is given by:

$$\dot{f}^{\mathrm{n}} = A_{\mathrm{N}}\dot{e}^{\mathrm{p}}, \quad A_{\mathrm{N}} = A_{\mathrm{N}}(e^{\mathrm{p}}) = \frac{f_{\mathrm{N}}}{S_{\mathrm{N}}\sqrt{2\pi}}\exp\left[-\frac{1}{2}\left(\frac{e^{\mathrm{p}} - e^{\mathrm{p}}_{\mathrm{N}}}{S_{\mathrm{N}}}\right)^{2}\right] \tag{3.9}$$

where the material parameters are: f_N nucleated void volume fraction, S_N standard deviation of the distribution of the nucleated voids and e^pN mean equivalent plastic strain at the incipient nucleation [17].
The void growth due to hydrostatic stresses is given by:

$$\dot{f}^{\mathrm{g}}_{\mathrm{hyd}} = (1 - f)\,\mathrm{tr}(\mathbf{D}^{\mathrm{p}}) \tag{3.10}$$

The void growth due to shear stress is:

$$\dot{f}^{\mathrm{g}}_{\mathrm{shr}} = k_{\mathrm{w}} f \frac{w\left(\mathrm{dev}\left[\mathbf{T}\right]\right)}{\sigma_{\mathrm{eq}}}\mathrm{dev}\left[\mathbf{T}\right] : \mathbf{D}^{\mathrm{p}} \tag{3.11}$$

according to [6]. Here, k_w is a material parameter and $w(\mathrm{dev}[\mathbf{T}])$ is a stress dependent function depending on the third invariant of the deviatoric stress tensor J_3 as follows:

$$w\left(\mathrm{dev}\left[\mathbf{T}\right]\right) = 1 - \left(\frac{27 J_3}{2\sigma_{\mathrm{eq}}^3}\right)^2 \tag{3.12}$$

The factor inside the eq. 3.12 is known as the Lode angle parameter ξ. The Lode angle θ distinguishes the stress state between axisymmetric and shear stress state. It is related to the normalized third deviator stress invariant J_3 as follows [18]:

$$\xi = \frac{27}{2}\frac{J_3}{\sigma_{\mathrm{eq}}{}^3} = \cos\left(3\theta\right) \tag{3.13}$$

For further details of the model regarding nucleation of the voids and the growth due to hydrostatic stresses, model implementation and related model parameters readers are referred to [19].

Enhanced Lemaitre Model

Similar to the Gurson type models with the void volume fraction, the effect of ductile damage is considered by the damage variable $D \in [0,1]$. It accounts for the deterioration of the load bearing capacity due to the evolution of the defect structure. The effective stress $\tilde{\mathbf{T}} = \mathbf{T} / (1 - D)$ represents the stress acting on the fictitious undamaged area, as opposed to the stress $\mathbf{T}$ acting on the total area. The plastic potential is given by $\Phi^{\mathrm{p}}(\mathbf{T}, q, D) = \tilde{\sigma}_{\mathrm{eq}} - q = \sqrt{3/2\ \mathrm{dev}(\tilde{\mathbf{T}}) : \mathrm{dev}(\tilde{\mathbf{T}})} - q$, where $\tilde{\sigma}_{\mathrm{eq}}$ represents the effective equivalent stress. The damage potential

$$\Phi^{\mathrm{d}} = \frac{S}{(\delta+1)}\left\langle\frac{Y - Y_0}{S}\right\rangle^{\delta+1}\frac{1}{(1-D)^{\beta}} \tag{3.14}$$

depends on the driving force $Y := Y^+$ and the material parameters S, β, δ and Y_0. $\langle x\rangle = (|x| + x)/2$ represents the Macauley bracket. In the context of blanking simulations it is important to consider that the evolution of damage under compressive stress states is different than under tensile stress states. Therefore, the weighting factor h is introduced

$$Y^+ = \frac{1+\nu}{2E}\left\{\sum_{i=1}^{3}\left[\left\langle\tilde{T}_i\right\rangle^2 + h\left\langle-\tilde{T}_i\right\rangle^2\right]\right\} - \frac{9\nu}{2E}\left\{\sum_{i=1}^{3}\left[\left\langle\tilde{p}\right\rangle^2 + h\left\langle-\tilde{p}\right\rangle^2\right]\right\} \tag{3.15}$$

to consider the effect of compressive stress states on the driving force. Here, $\tilde{T}_i$ represent the principle stresses of $\tilde{\mathbf{T}}$ and $\tilde{p} := 1/3\ \mathrm{tr}(\tilde{T})$ the hydrostatic pressure. Differentiation of (3.14), with respect to Y reveals the particular form of the damage evolution

$$\dot{D} = \lambda\left\langle\frac{Y - Y_0}{S}\right\rangle^{\delta}\frac{1}{(1-D)^{\beta}} \tag{3.16}$$

The model is implemented via the user material interface into Abaqus/Explicit. For details of

the model formulation and the implementation the reader is referred to [9]. The standard damage model of Lemaitre [3] does not distinguish between compressive stresses and tensile stresses for the evolution of damage. This is in contrast to experimental observations, e.g. of Bao et al. [20], such as a cut-off value of the stress triaxiality -1/3, below which fracture does not occur. With the original Lemaitre model, i.e. $h = 1$ in (3.14), one obtains a fracture curve which does not consider the sign of triaxiality. In general, for technical metals, fracture occurs at higher strains for compressive stresses. Thus the fracture strain for η = -1/3 tends asymptotically to infinity in the current model for the limiting case of $h = 0$.

In order to modify the cumulative damage for Lemaitre Model according to the shear stress states, the shear fracture related parameter of the fracture model in [21] is introduced to the damage evolution rate of the model. Then the damage evolution equation in eq. 3.15 reads:

$$\dot{D} = \lambda \left(\frac{2\tau_{\max}}{\sigma_{eq}} \right)^{\kappa} \left\langle \frac{Y - Y_0}{S} \right\rangle^{\delta} \frac{1}{\left(1 - D\right)^{\beta}} \tag{3.17}$$

The relation between selected factor and Lode angle θ can be shown as [22]:

$$\frac{2\tau_{\max}}{\sigma_{eq}} = \frac{2}{3}\left(\cos\theta - \cos\left(\frac{4}{3}\pi - \theta \right) \right) \tag{3.18}$$

3.2 Modelling of experiments

All experiments (i.e. notched tensile test, biaxial Nakajima test and blanking process) are modelled in the commercial software Abaqus/Explicit with a VUMAT implementation of the described material models. Failure of the material is represented by the deletion of those elements, at which the void volume fraction f, or the damage variable D reaches the critical value f_f, or D_c respectively.

The blanking process was simulated using a two-dimensional axisymmetric model with bilinear CAX4R elements. The mesh size in the process zone is set to 25 µm and maintained constant with an Arbitrary-Lagrange-Euler (ALE) approach (Figure 2). Punch and die are modelled as rigid bodies.

The notched tensile test and biaxial Nakajima test are modelled in 3D space using trilinear C3D8R elements. For the notched specimen all three symmetry planes are used and for the Nakajima specimen a quarter model is used. The mesh size of the models for parameter identification is taken as 1 mm. Because the required mesh size for the blanking process is much finer than this value, one of the model parameters, S for Lemaitre model and k_w for Gurson Model are manually scaled for the mesh size of 25 µm. The model parameters for the mesh size of 25 µm are tabulated in Table 3.

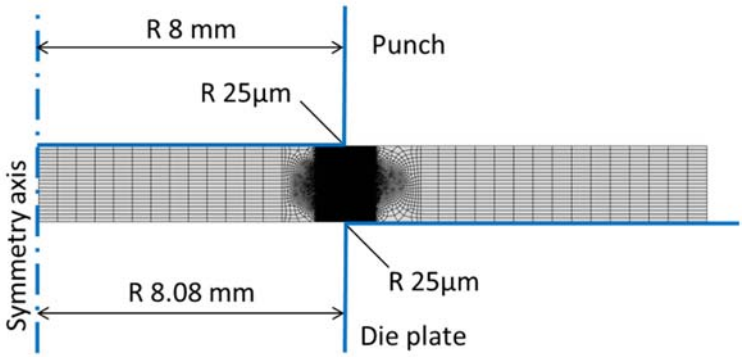

Figure 2: Simulation model of the blanking process.

3.3 Parameter identification strategy

The parameters for the elasto-plastic regime are obtained directly from uniaxial tensile test (Table 1). For the parameters related to material softening a distinction of cases is necessary. Parameter of the Gurson model are determined predominantly directly from microscopic analysis. Yet some parameters need to be identified inversely. The parameter related to void growth due to shear k_w (cf. eq. 3.10) is obtained a posteriori by fitting to the force displacement curve of the blanking process.

In the case of Lemaitre's model all parameters related to softening (i.e. S, β, δ, κ and Y_0) have to be identified by an inverse strategy. The critical damage D_c may be determined a posteriori. For the inverse identification the force displacement curve of the notched tensile and biaxial Nakajima test are used. The target function

$$e = \sum_{i=1}^{N} \sqrt{\left(F(u_i)_{\exp}^{R10} - F(u_i)_{sim}^{R10} \right)^2} + \sum_{i=1}^{N} \sqrt{\left(F(u_i)_{\exp}^{G0} - F(u_i)_{sim}^{G0} \right)^2} \tag{3.19}$$

needs to be minimized. $F(u_i)$ is the force vector with respect to the displacement. R10 denotes the notched tensile test and G0 the Nakajima test. The identification optimization itself is performed manually. The parameters for both models are tabulated in Table 2.

4 RESULTS

In the context of blanking special attention must be paid to use material models which are appropriate to treat evolution of material degradation with respect to all of the occurring stress states. The application to blanking is a challenging task, one of the reasons being that the triaxiality η takes values between - 2/3 and + 2/3 for a closed cut line [10]. The representatives of both model families should be able to account for these stress states. Therefore it is expected that the comparison is fair.

The simulations of both models yield a fair prediction of force-displacement curve. The solution of the Lemaitre model is very close to the experimental measured one. The deviation in maximum force is less than 2%. The results of the Gurson model are significantly improved compared to the previous study of Hambli [5].

Table 2: Identified material parameters for both models.

Enhanced Gurson model [15], [16], [12]									
f_0	q_1	q_2	q_3	f_N	s_N	e^p_N	f_c	f_f	k_w
0.0008	1.5	1.0	2.25	0.00062	0.1283	0.5421	0.015	0.07	1.2

Enhanced Lemaitre model						
Y_0 in MPa	S in MPa	β	δ	κ	h	D_c
1.06	6	15	2	1	0	0.2

This is probably due to the enhancement for shear activated void growth. Yet the solution accuracy is lower than for the enhanced Lemaitre model. The maximum force predicted is 4.4% below the maximum force in experiment. Despite these results the Gurson model predicts the onset of the first crack very well, with respect to both punch displacement and place of initiation (Figure 3).

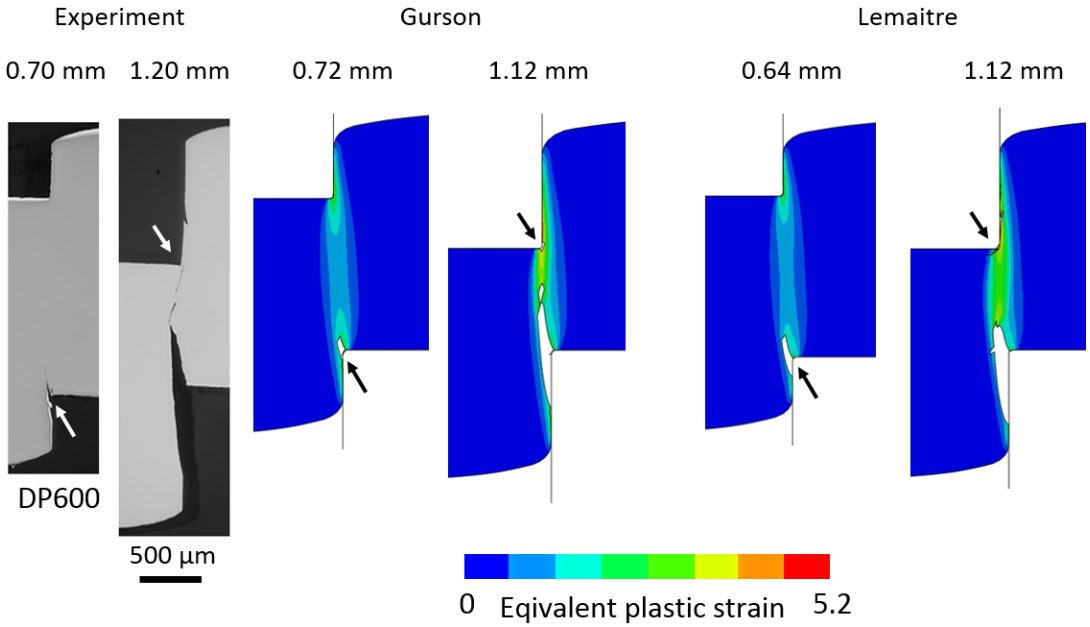

Figure 3: Occurence of initial crack and total rupture. Experiment and results for Gurson model from [7].

The Lemaitre model also predicts the place of initiation correctly on the lower side of blank, but the punch displacement for this event is predicted too early and slightly worse than with the Gurson model. Prediction of the second cracking from the upper side of the blank is achieved with both models similarly well.

5 CONCLUSION

Two modern implementations of different continuum damage mechanics models have been applied to a complex process simulation. Parameters for the Gurson model have been identified

predominantly with a scanning electron microscope, while parameters for Lemaitre have been identified completely by an inverse strategy. Both models have shown good prediction accuracy. On the one hand the Lemaitre model predicted the punch force during the process almost excellently, on the other hand the Gurson model yielded better results for predicting the onset of damage, which is important for determining the amount of burnish and fracture on the cut surface.

Concerning the effort of parameter identification the inverse strategy is considerably superior. At first the preparation of samples for SEM in order to observe voids in the nanometer scale is time consuming. Secondly, it takes a lot of time for the user of SEM to distinguish voids from other artefacts. In contrast the experiments for inverse strategy can be conducted easily. Due to the short simulation time of these experiments (one Nakajima simulation needed roughly two hours) the parameters could be identified manually. If the inverse identification were run automated as presented in [10] the complete procedure would probably have needed between one and four days, depending on the number of used computing cores.

On the other hand the processing of microscope images might be automated at least partially, as well. Moreover, the Gurson's model reveals quantities (e.g. void volume fraction) directly comparable to microstructural information. This information might give a better insight in the physics on microstructure level and will be used in future validations.

ACKNOWLEDGEMENT

The authors gratefully acknowledge funding by the German Research Foundation (DFG) within the scope of the Transregional Collaborative Research Centre on sheet-bulk metal forming (SFB/TR 73) in the project C4 'Analysis of load history dependent evolution of damage and microstructure for the numerical design of sheet-bulk metal forming processes'.

Furthermore, the authors would like to thank Florian Nürnberger and Gregory Gerstein for optical as well as scanning electron microscopy and corresponding discussions.

REFERENCES

1. Gurson, A.L., *Continuum Theory of Ductile Rupture by Void Nucleation and Growth .1. Yield Criteria and Flow Rules for Porous Ductile Media.* Journal of Engineering Materials and Technology-Transactions of the Asme, 1977. **99**(1): p. 2-15.
2. Tvergaard, V. and A. Needleman, *Analysis of the Cup-Cone Fracture in a Round Tensile Bar.* Acta Metallurgica, 1984. **32**(1): p. 157-169.
3. Lemaitre, J., *A Continuous Damage Mechanics Model for Ductile Fracture.* Journal of Engineering Materials and Technology-Transactions of the Asme, 1985. **107**(1): p. 83-89.
4. Vaz, M., et al., *Considerations on parameter identification and material response for Gurson-type and Lemaitre-type constitutive models.* International Journal of Mechanical Sciences, 2016. **106**: p. 254-265.
5. Hambli, R., *Comparison between Lemaitre and Gurson damage models in crack growth simulation during blanking process.* International Journal of Mechanical Sciences, 2001. **43**: p. 2769-2790.
6. Nahshon, K. and J.W. Hutchinson, *Modification of the Gurson Model for shear failure.* European Journal of Mechanics a-Solids, 2008. **27**(1): p. 1-17.
7. Isik, K., et al. *Investigations of ductile damage in DP600 and DC04 deep drawing steel sheets during punching*. in *21st European Conference on Fracture (ECF21)*. 2016. Catania, Italy: Procedia Structural Integrity.
8. Desmorat, R. and S. Cantournet, *Modeling microdefects closure effect with isotropic/anisotropic damage.* International Journal of Damage Mechanics, 2008. **17**(1): p. 65-96.

9. Soyarslan, C. and A.E. Tekkaya, *A damage coupled orthotropic finite plasticity model for sheet metal forming: CDM approach (vol 48, pg 150, 2010).* Computational Materials Science, 2010. **48**(4): p. 875-876.
10. Gutknecht, F., et al. *Advanced material model for shear cutting of metal sheets*. in *COMPLAS XIII*. 2015. Barcelona, Spain: CIMNE.
11. Gerstein, G., et al., *The effect of texture in modeling deformation processes of bcc steel sheets.* Materials Letters, 2016. **164**: p. 356-359.
12. Isik, K., et al., *Evaluation of Void Nucleation and Development during Plastic Deformation of Dual-Phase Steel DP600.* steel research international, 2016. **87**(12): p. 1583-1591.
13. Lee, E.H., *Elastic-Plastic Deformation at Finite Strains.* Journal of Applied Mechanics, 1969. **36**(1): p. 1-&.
14. Clausmeyer, T. and B. Svendsen, *Comparison of two models for anisotropic hardening and yield surface evolution in bcc sheet steels.* European Journal of Mechanics - A/Solids, 2015. **54**: p. 120-131.
15. Tvergaard, V., *Influence of Voids on Shear Band Instabilities under Plane-Strain Conditions.* International Journal of Fracture, 1981. **17**(4): p. 389-407.
16. Tvergaard, V., *On Localization in Ductile Materials Containing Spherical Voids.* International Journal of Fracture, 1982. **18**(4): p. 237-252.
17. Chu, C.C. and A. Needleman, *Void Nucleation Effects in Biaxially Stretched Sheets.* Journal of Engineering Materials and Technology-Transactions of the Asme, 1980. **102**(3): p. 249-256.
18. Bai, Y.L. and T. Wierzbicki, *Application of extended Mohr-Coulomb criterion to ductile fracture.* International Journal of Fracture, 2010. **161**(1): p. 1-20.
19. Soyarslan, C., et al., *An Experimental and Numerical Assessment of Sheet-Bulk Formability of Mild Steel DC04.* Journal of Manufacturing Science and Engineering-Transactions of the Asme, 2011. **133**(6).
20. Bao, Y. and T. Wierzbicki, *On fracture locus in the equivalent strain and stress triaxiality space.* International Journal of Mechanical Sciences, 2004. **46**(1): p. 81-98.
21. Isik, K., et al., *Enhancement of Lemaitre Model to Predict Cracks at Low and Negative Triaxialities in Sheet Metal Forming.* Key Engineering Materials, 2015. **639**: p. 427-434.
22. Lou, Y., et al., *New ductile fracture criterion for prediction of fracture forming limit diagrams of sheet metals.* International Journal of Solids and Structures, 2012. **49**(25): p. 3605-3615.